

Supporting Information

Stimuli-Responsive Degrafting of Polymer Brushes via Addressable Catecholato-Metal Attachments

Asger Holm Agergaard^{a,b}, Steen Uttrup Pedersen^{a,b}, Henrik Birkedal^{a,b,*} and Kim Daasbjerg^{a,b,*}

^a*Department of Chemistry, Aarhus University, Langelandsgade 140, Aarhus C DK-8000, Denmark*

^b*Interdisciplinary Nanoscience Center (iNANO) Aarhus University, Gustav Wieds Vej 14, Aarhus C DK-8000,
Denmark*

Materials and Methods

Chemicals. α -Bromoisobutyryl bromide (BiBB, 98%), 2,2'-bipyridyl (>99 %), sodium ascorbate (>99 %), triethylamine (>99%), 4-nitrocatechol (97%), sodium nitrite (>99%), $\text{AlCl}_3 \cdot 6\text{H}_2\text{O}$ (97%), $\text{CuCl}_2 \cdot 2\text{H}_2\text{O}$ (99%, Merck), $\text{FeCl}_3 \cdot 6\text{H}_2\text{O}$ (>99%, Riedel de Haën), sodium acetate trihydrate (Bie & Berntsen), dopamine hydrochloride, dichloromethane, acetonitrile, pentane, methanol, ethanol, and acetone were obtained from Sigma Aldrich, unless otherwise noted, and used as received. Methyl methacrylate (99%, ≤ 30 ppm 4-methoxyphenol as inhibitor) was sequentially washed with 2 M NaOH and Milli-Q water, dried with Na_2SO_4 and distilled under reduced pressure at 40 °C to remove 4-methoxyphenol. Tetrabutylammonium tetrafluoroborate (Bu_4NBF_4) was synthesized according to a previously reported procedure.^{S1}

Substrates. Glassy carbon (GC) rods (Sigradur G, HTW, $\phi = 1$ mm) embedded in epoxy resin and GC plates (Sigradur G, HTW, 10 mm \times 10 mm \times 1 mm) were used as working electrode substrates. The rod electrodes were polished using 9, 3, 1, and 0.25 μm polishing cloths (Struers) with corresponding diamond pastes (Struers), and subsequently cleaned by ultrasonication in acetone (HPLC grade). GC plates were ultrasonicated for 10 min in Milli-Q water, acetone (HPLC grade), and pentane prior to use.

Surface Modification

Catechol was grafted to GC or Quartz Crystal Microbalance working electrodes in a standard three-electrode setup by grafting of catechol diazonium ions formed in-situ, using a procedure similar to that reported by Henderson et al.^{S2} The electrochemical cell contained 4-nitrocatechol (2 mM) and sodium nitrite (8 mM) in 1 M HCl under an Ar atmosphere. When modifying QCM sensors, a metal ion was added in a 20 mM concentration to prevent the diol from forming bidentate coordination bonds to the surface. QCM sensors needed for experiments with Al^{3+} were grafted under the presence of Al^{3+} ions and vice versa for QCM sensors used in experiments with Fe^{3+} . The electrodes were modified by electrolysis for 5 min at -0.7 V vs SCE and cleaned by ultrasonication in acetone (HPLC grade) to yield the catechol modified substrates (GC_{Cat}). QCM sensors were furthermore cleaned by ultrasound in 1 M HCl. Metal ions were introduced to the surface by submerging GC_{Cat} in an aqueous solution of $\text{AlCl}_3 \cdot 6\text{H}_2\text{O}$ (20 mM) or $\text{FeCl}_3 \cdot 6\text{H}_2\text{O}$ (20 mM) for 5 min and rinsing with Milli-Q water and acetone (HPLC grade). The $\text{GC}_{\text{Cat-Al}}$ or $\text{GC}_{\text{Cat-Fe}}$ samples thus obtained were subsequently submerged in an Ar purged, buffered, aqueous solution of dopamine (10 mM) at various pH levels for 10 min and rinsed with acetone to afford $\text{GC}_{\text{Cat-Dopa}}$.

The ATRP initiator was immobilized on the surface by submerging $\text{GC}_{\text{Cat-Dopa}}$ in an Ar purged solution of BiBB (0.5 M) and Et_3N (0.05 M) in CH_2Cl_2 for 3 h on a shaker board. Substrates were cleaned by

ultrasonication in CH_2Cl_2 and acetone (HPLC grade) yielding $\text{GC}_{\text{Cat-In}}$. Polymer brushes were synthesized in the following way: A solution of methyl methacrylate (1 M) in a 1:1 (v:v) mixture of Milli-Q water and MeOH was purged with Ar. After purging, $\text{CuCl}_2 \cdot 2\text{H}_2\text{O}$ (4 mM), 2,2'-bipyridyl (8 mM) and sodium ascorbate (3.5 mM) were added. The vessel was placed on ice, and after 10 min the substrates were submerged and the reaction kept under an Ar atmosphere.^{S3} After 1 h, the samples were removed from the solution and rinsed in methanol and water followed by ultrasonication in acetone (HPLC grade) to obtain the $\text{GC}_{\text{Cat-Dopa-PMMA}}$ substrates.

Quartz Crystal Microbalance

All measurements were carried out using a Q-Sense Analyzer unit, recording both frequency and dissipation. In short, experiments were carried out using catechol-modified gold QCM-sensors (5 MHz, Biolin Scientific QSX 301). All measurements were carried out under constant flow at a rate of 100 $\mu\text{L}/\text{min}$. First, a stable frequency baseline was obtained using pure Milli-Q water. Then, a 20 mM solution of either $\text{AlCl}_3 \cdot 6\text{H}_2\text{O}$ or $\text{FeCl}_3 \cdot 6\text{H}_2\text{O}$ was flowed through the chamber, resulting in catecholato-metal complexes on the surface, evidenced by a decrease in resonance frequency. Subsequently, argon purged solutions of phosphate buffers containing 1 mM dopamine were passed through the chamber, and the change in frequency recorded. From the change in frequency of the 3rd overtone, the adsorbed mass was obtained through the Sauerbrey equation, using a Sauerbrey constant of 17.7 $\text{ng cm}^{-2} \text{Hz}^{-1}$.

Electrochemical response of grafted catechol

Cyclic voltammetry of grafted catechol. GC_{Cat} rod electrodes were used as working electrodes in a three-electrode setup in 0.1 M sodium acetate/(9:1 $\text{H}_2\text{O}/\text{acetonitrile}$). A Pt wire served as counter electrode and SCE as reference electrode.

Repeated release of metal ions from $\text{GC}_{\text{Cat-M}}$. $\text{GC}_{\text{Cat-M}}$ rod electrodes served as working electrodes in a three-electrode setup in 0.1 M sodium acetate/(9:1 $\text{H}_2\text{O}/\text{acetonitrile}$). To unload metal ions from $\text{GC}_{\text{Cat-Al}}$ under oxidative conditions, cyclic voltammograms were recorded from -0.1 – 0.45 V vs SCE using $\nu = 0.1$ V s^{-1} . For each cycle, $E_{\text{p,a}}$ was measured. Ions were repeatedly loaded into the sample using the dipping procedure previously described. For the release from $\text{GC}_{\text{Cat-Fe}}$, a 30 s oxidative pulse at 0.7 V vs. SCE was utilized under the same conditions.

Oxidative removal of polymer brushes from $\text{GC}_{\text{Cat-PMMA}}$. Plates of $\text{GC}_{\text{Cat-PMMA}}$ served as working electrodes in a three-electrode setup in 0.1 M $\text{Bu}_4\text{NBF}_4/\text{acetonitrile}$. The samples were subjected to three potential cycles from 0.1–1.4 V vs SCE followed by a chronocoulometric oxidation at 0.8 V SCE for 30 s. Finally, the samples were sonicated in acetone.

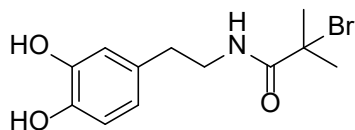
Surface Characterization Techniques

X-ray photoelectron spectroscopy (XPS). X-ray photoelectron spectroscopy (XPS) was measured with a Kratos Axis Ultra-DLD instrument using a monochromatic Al K α X-ray source at a power of 150 W. The pressure in the chamber was kept below 5×10^{-9} mbar during measurements. Full survey spectra were obtained with a pass energy of 120 eV, while the pass energy for high resolution spectra was 20 eV. An electron flood gun was used for sample neutralization. The spectra were calibrated against the C 1s signal at 285.0 eV, and processed in CasaXPS. High resolution spectra were fitted with an asymmetric line shape consisting of a Lorentzian line shape convoluted by a Gaussian line shape, generated by the CasaXPS software.

Ellipsometry. Measurements were taken using a rotating analyzer ellipsometer (EL X-02C, Dre, Germany) with a He-Ne laser (632.8 nm). The angle of laser incidence was 65°. The phase difference (Δ) and the amplitude ratio upon reflection (Ψ) of clean substrates and in between each modification step was measured and processed in the Ellips32 software. The software calculated the complex refractive index of the bare surface, while a 3-layer optical model was used for the modified samples. A refractive index of 1.55 for the organic film was assumed, independent of thickness, for modified samples. Measurements were taken three times in three different locations on each substrate and data presented are average values.

Infrared reflection absorption spectroscopy (IRRAS). Measurements were made on a Nicolet 6700 FTIR spectrometer coupled to an external Varian Experiment Module with a narrow band Mercury-Cadmium-Telluride-detector cooled with liquid nitrogen. The angle of incidence was 60°, the spectral resolution was 4 cm⁻¹, and 200 scans were averaged for each spectrum. Measurements were carried out in an atmosphere of dry air at room temperature. The logarithm of the p-polarized reflectivity of the film divided by the reflectivity of the bare substrate was presented as IRRAS absorbance.

Synthesis of 2-bromo-N-(3,4-dihydroxyphenethyl)-2-methylpropanamide



10 ml MeOH was placed in a 25-mL round-bottomed flask and degassed with Ar for 10 min. Dopamine hydrochloride (1 g, 5.25 mmol, 1 equiv) was added and dissolved, followed by Ar purging in 10 min. Et₃N (0.73 ml, 5.25 mmol, 1 equiv) was added and the temperature held at 0 °C. Two other solutions were prepared where α -bromoisobutyryl bromide (0.65 ml, 5.25 mmol, 1 equiv) was dissolved in 2 ml tetrahydrofuran and triethylamine (1.1 ml, 1.5 equiv) in 2 ml MeOH. Both these solutions were added dropwise to the round-bottomed flask and the reaction was left for 1 h. The solvent was removed under

vacuum and the crude was redissolved in 25 ml chloroform and washed sequentially with 1 M HCl, Milli-Q, and brine before drying in vacuo over night to give a clear, viscous oil. Yield = 0.79 g (50%). ^1H NMR (400 MHz, CDCl_3): δ 8.75 (bs, 1H), 8.65 (bs, 1H), 8.1 ppm (t, $J = 5.5$ Hz, 1H), 6.62 ppm (d, $J = 8$ Hz, 1H), 6.43 ppm (dd, $J = 8$ Hz, 2 Hz, 1H), 6.57 ppm (d, $J = 2$ Hz, 1H), 3.20 ppm (q, $J = 6$ Hz, 9 Hz, 2H), 2.53 ppm (t, $J = 8$ Hz, 2H), 1.83 ppm (s, 6H).

Results

QCM Data for dopamine binding onto a catecholato- Al^{3+} modified QCM sensor Figure S1 shows the data for dopamine binding to catecholato- Al^{3+} complexes on an Au QCM sensor.

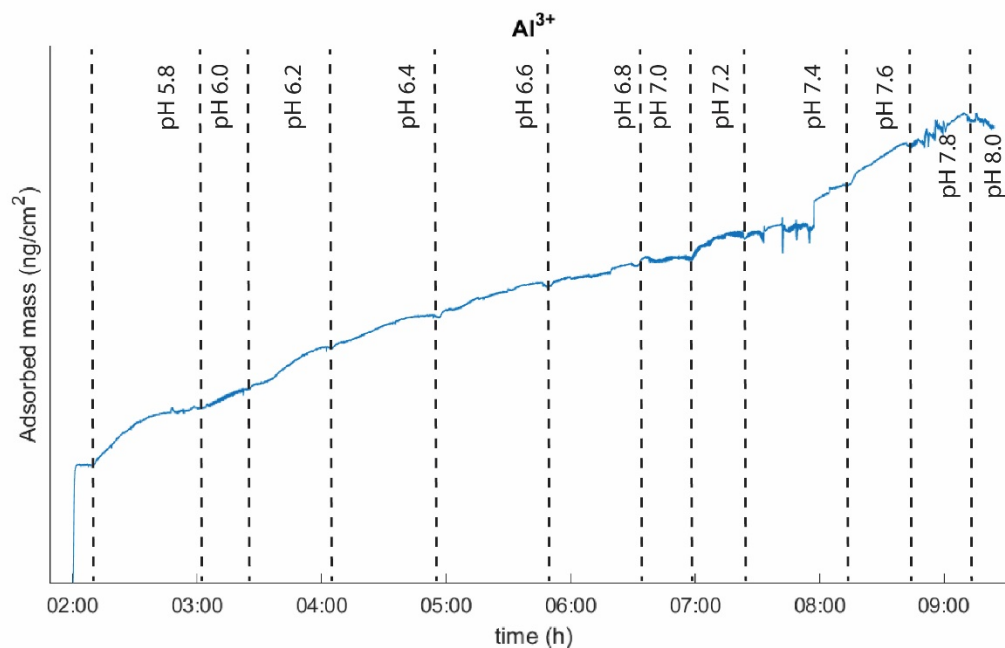


Figure S1. Adsorbed mass on a catecholato- Al^{3+} grafted QCM sensor in a 1 mM dopamine solution vs. time. Dotted lines indicate change in pH value according to the shown value. Around 08:00 hours, an air bubble entered the system, resulting in the jump in frequency observed during the pH 7.4 phase of the experiment. The data was corrected for this jump prior to reporting.

The raw data for phosphate adsorption on a catecholato- Al^{3+} modified QCM sensor is shown in Figure S2.

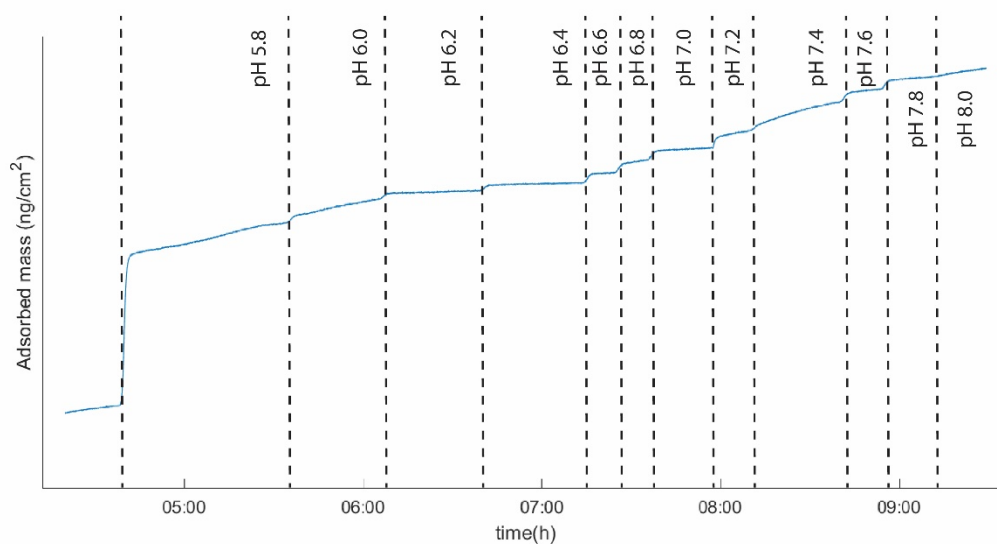


Figure S2. Adsorbed mass on a catecholato- Al^{3+} grafted QCM sensor in buffered phosphate solutions.

Data for dopamine binding onto a catecholato- Fe^{3+} modified QCM sensor Figure S3 shows a representative set of raw data for dopamine binding to catecholato- Fe^{3+} complexes on an Au QCM sensor. Dotted lines indicate change in pH value of the phosphate solution used.

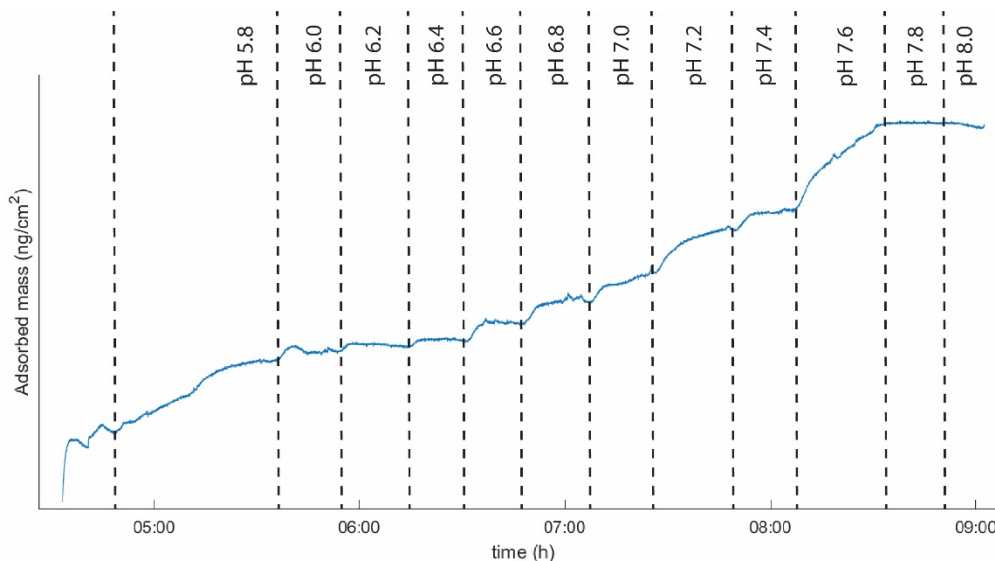


Figure S3. Adsorbed mass on a catecholato- Fe^{3+} grafted QCM sensor in a 1 mM dopamine solution vs. time. Dotted lines indicate change in pH value according to the shown value.

Figure S4 shows the adsorbed mass on a catecholato- Fe^{3+} modified QCM sensor as a function of pH, when dopamine is present in solution.

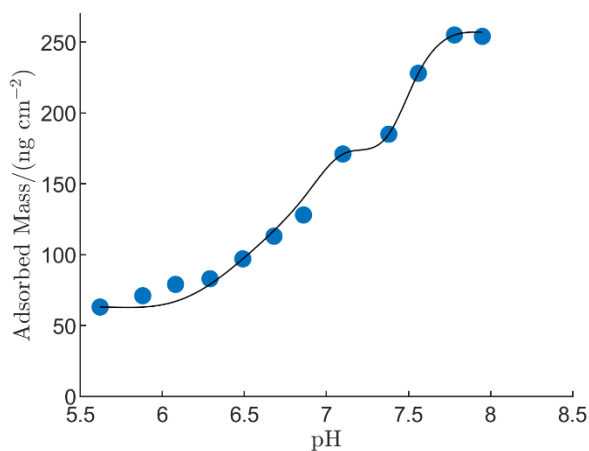


Figure S4. Adsorbed mass from Figure S3 as a function of pH in the dopamine solution. Adsorbed mass is reported relative to that adsorbed in pure phosphate buffer at pH 5.8. Line to guide the eye.

C 1s high-resolution (HR) XPS spectra of bare GC, GC_{Cat} , $\text{GC}_{\text{Cat-Dopa}}$, $\text{GC}_{\text{Cat-In}}$. XPS spectra of the C 1s region reveal the introduction of the grafted catechol in GC_{Cat} , followed by introduction of dopamine in $\text{GC}_{\text{Cat-Dopa}}$, and the subsequent change in the local electronic environment of C-N on going from amine to amide in the formation of $\text{GC}_{\text{Cat-In}}$.

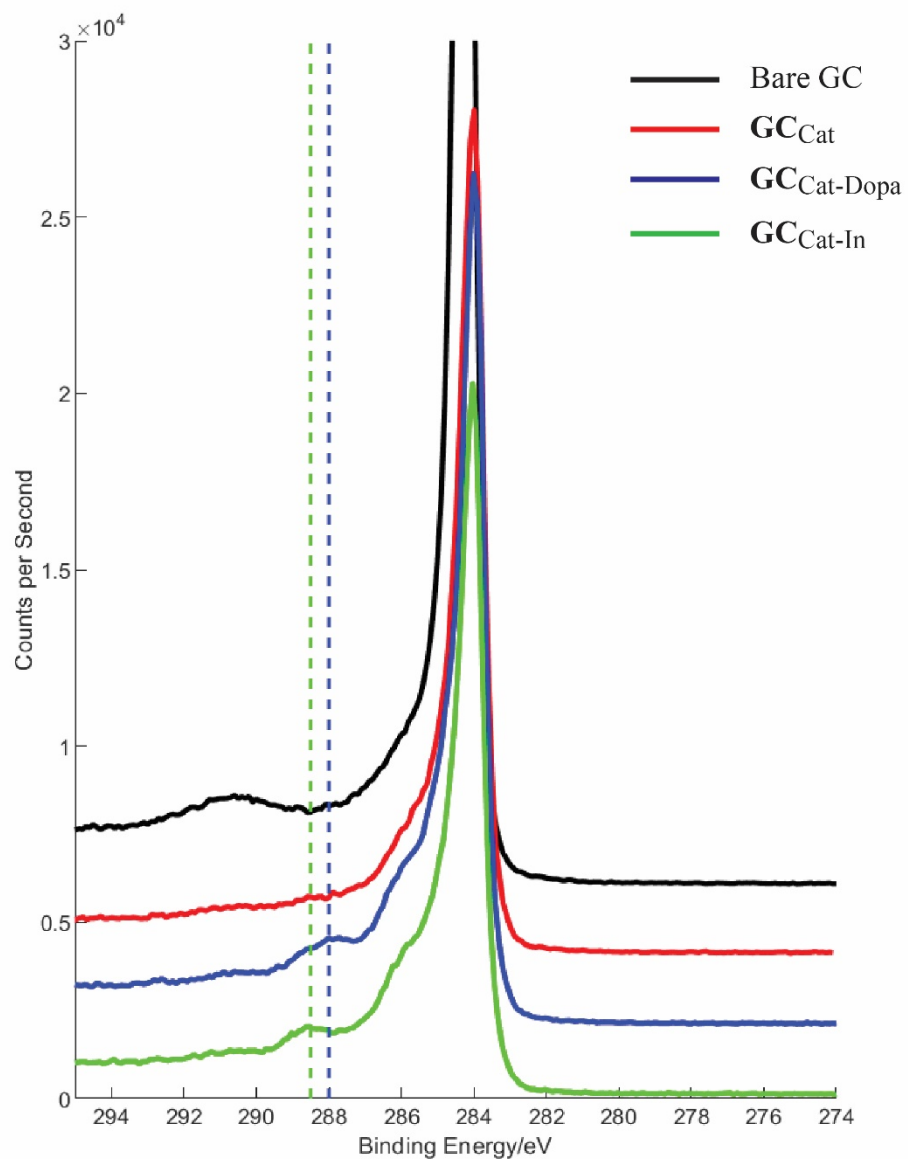


Figure S5. HR-XPS of the C 1s region of a bare GC (black), GC_{Cat} (red), $\text{GC}_{\text{Cat-Dopa}}$ (blue), and $\text{GC}_{\text{Cat-In}}$ (green).

Cyclic Voltammetry of grafted catechol on GC_{Cat}. Figures S6 and S7 show the cyclic voltammograms recorded at various sweep rates to deduce the electron transfer characteristics at **GC_{Cat}**.

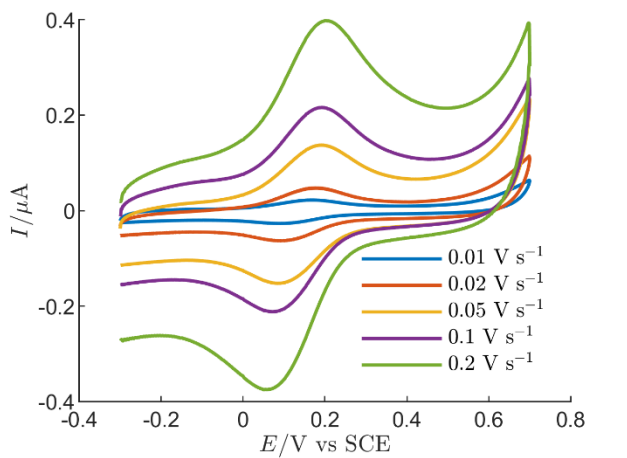


Figure S6. Cyclic voltammograms of grafted catechol recorded on **GC_{Cat}** in 0.1 M sodium acetate/(9:1 H₂O/acetonitrile).

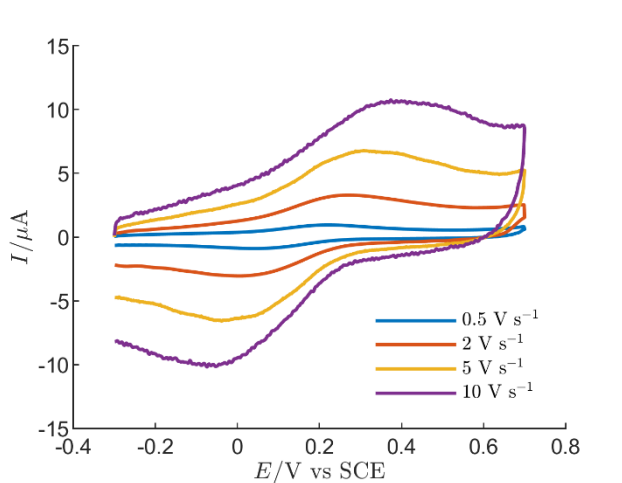


Figure S7. Cyclic voltammograms of grafted catechol recorded on **GC_{Cat}** in 0.1 M sodium acetate/(9:1 H₂O/acetonitrile).

Analysis of cyclic voltammetry of grafted catechol on GC_{Cat}. The anodic ($i_{p,a}$) and cathodic ($i_{p,c}$) peak currents (obtained from Figures S6 and S7) were plotted against $\log v$ and fitted with a linear relation. The slopes of 0.89 and 0.86, respectively, are slightly smaller than 1, indicating that the grafted catechol obeys near-Nernstian electrode behaviour.

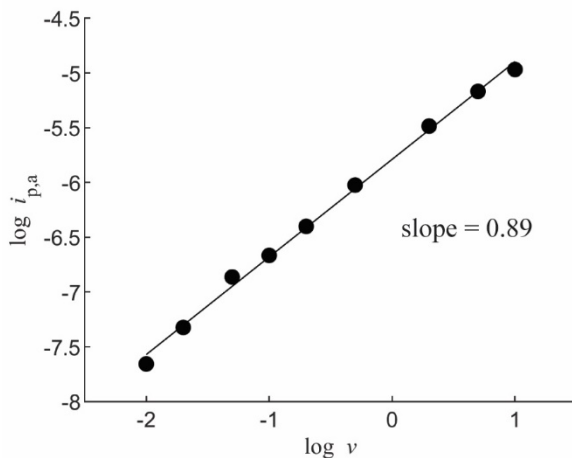


Figure S8. $\log i_{p,a}$ of grafted catechol on GC_{Cat} plotted against $\log v$.

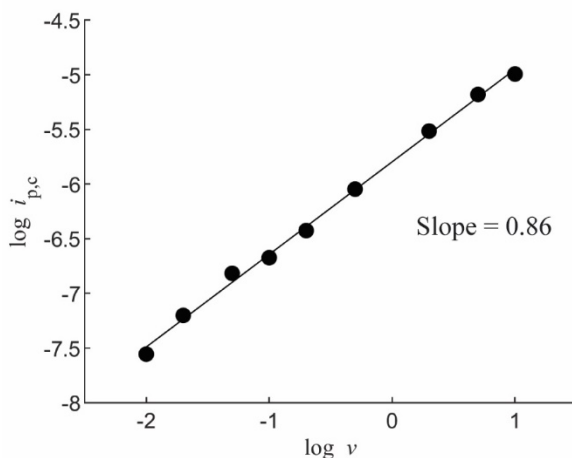


Figure S9. $\log i_{p,c}$ of grafted catechol on GC_{Cat} plotted against $\log v$.

Coverage of electroactive catechol. To determine the coverage of electroactive catechol units, the oxidation peak in the cyclic voltammograms (Figures S6 and S7) was baseline corrected (see Figure S10). The total charge transferred in the oxidation was obtained through the following relation $Q = \frac{1}{v} \int i(E)dE$ where v is the sweep rate, Q is the faradaic charge transferred, i is the current, and E the potential. Finally, the coverage of electroactive catechol moieties, Γ_{Cat} , was obtained through $\Gamma_{\text{Cat}} = \frac{Q}{A \cdot F}$, where A was the electrode area,

and F was Faradays constant. The presented value is the mean value calculated for all voltammograms recorded.

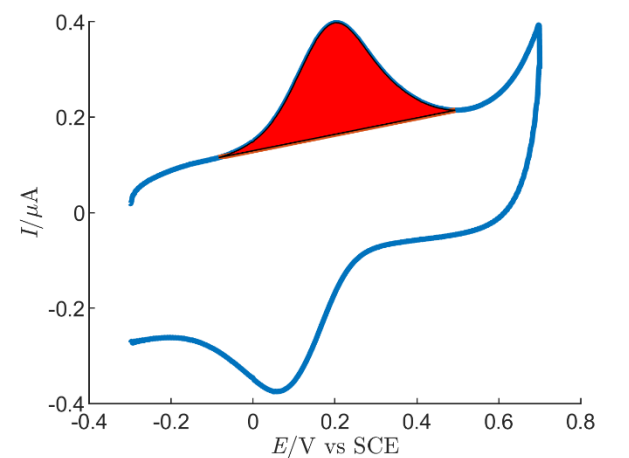


Figure S10. Baseline correction and integrated area of a cyclic voltammogram measured on GC_{Cat} at $\nu = 0.2 \text{ V}\cdot\text{s}^{-1}$, to determine the surface coverage of active catechol.

Apparent heterogeneous rate constant (k_s). To determine k_s for GC_{Cat} , the $E_{\text{p,a}}$ and $E_{\text{p,c}}$ values obtained from the cyclic voltammograms (Figures S6 and S7) were analyzed according to the appropriate formalism given by Laviron.^{S4} Plots of $E_p - E^0$ vs $\log \nu$ were constructed (Figure S11) with the formal electrode potential, E^0 , determined as the average of the peak potentials.

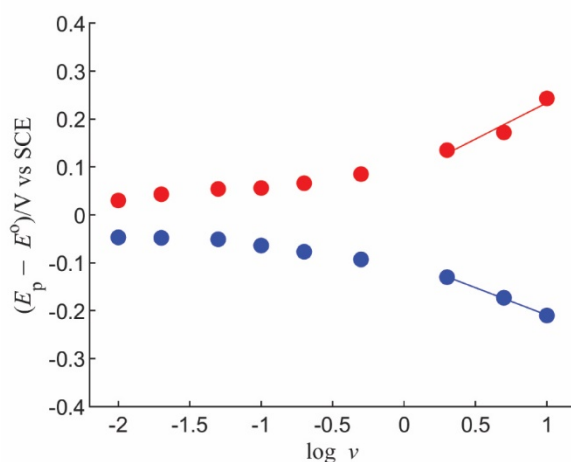


Figure S11. Plots of $E_{\text{p,a}} - E^0$ (red points) and $E_{\text{p,c}} - E^0$ (blue points) vs $\log \nu$. For data fulfilling $E_{\text{p,a}} - E_{\text{p,c}} > 200 \text{ mV}$, a linear fit is used to determine k_s .

For the sweep rates where $|E_{\text{p,a}} - E_{\text{p,c}}| > 200 \text{ mV}$ (valid for $\nu \geq 2 \text{ V s}^{-1}$), a linear fit was introduced. By extrapolating the linear regions of these plots to $E_{\text{p,a}} - E^0 = 0$ or $E_{\text{p,c}} - E^0 = 0$, the so-called critical sweep

rates, v_a and v_c , were obtained. On this basis the transfer coefficient, α , could be obtained through the relation $\frac{v_a}{v_c} = \frac{\alpha}{1-\alpha}$ and, in addition, k_s from eqs S1 and S2.

$$E_{p,c} = E^o - \frac{RT}{\alpha nF} \ln \left(\frac{\alpha nFv}{RTk_s} \right) \quad (S1)$$

$$E_{p,a} = E^o + \frac{RT}{(1-\alpha)nF} \ln \left(\frac{(1-\alpha)nFv}{RTk_s} \right) \quad (S2)$$

Note that n is the number of electrons involved in the electrode process ($n = 2$), while R , T , and F have their usual meanings. Under the given conditions ($E_{p,c} = E^o$ or $E_{p,a} = E^o$), k_s was obtained by combining eqs S1 and S2 to eq S3.

$$k_s = \frac{\alpha nFv_c}{RT} = \frac{(1-\alpha)nFv_a}{RT} \quad (S3)$$

In this manner, k_s was determined to 7.8 s^{-1} .

Repeated unloading and loading of Fe^{3+} from $\text{GC}_{\text{Cat-Fe}}$ The anodic peak potential of $\text{GC}_{\text{Cat-Fe}}$ was measured with cyclic voltammetry. Then, $\text{GC}_{\text{Cat-Fe}}$ was oxidized by a 30 s pulse at 0.7 V vs. SCE, rinsed in Milli-Q water and the anodic peak potential remeasured. The surface was then loaded with Fe^{3+} again, and the cycle repeated 7 times, with the anodic peak potentials shown in Figure S12. On average, the potential shift was 28 mV more positive upon binding Fe^{3+} .

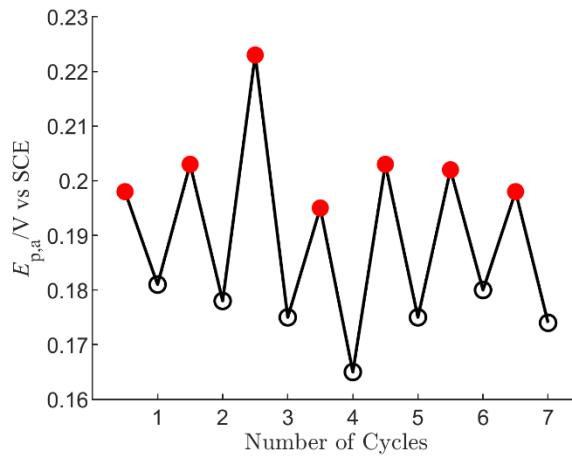


Figure S12. Repeated unloading and loading of Fe^{3+} from GC_{Cat} . Red points represent freshly Fe^{3+} loaded surfaces, while open circles represent the deloaded surface.

Cyclic voltammetry on $\text{GC}_{\text{Cat-PMMA}}$. Figure S13 shows that the current in the featureless cyclic voltammograms of $\text{GC}_{\text{Cat-PMMA}}$ is capacitive of nature. This can be attributed to the strongly blocking ability of the dense PMMA brush layer.

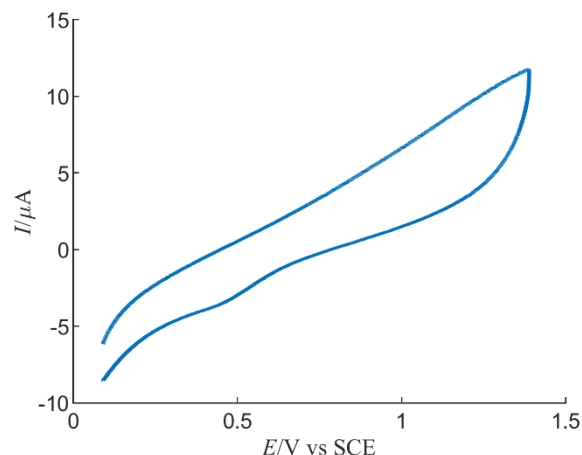


Figure S13. Cyclic voltammogram recorded on $\text{GC}_{\text{Cat-PMMA}}$ using $\nu = 0.1 \text{ V s}^{-1}$ in $0.1 \text{ M Bu}_4\text{NBF}_4/\text{acetonitrile}$.

Stability of $\text{GC}_{\text{Cat-PMMA}}$ toward sonication and heating. Figures S14 and S15 show the IRRAS spectra recorded of $\text{GC}_{\text{Cat-PMMA}}$ before and after 20 min ultrasonication in acetone or heating to $100 \text{ }^\circ\text{C}$ for 1 h respectively. With no significant changes observed in signal location or strength, it may be concluded that the brushes are left unaffected by the harsh treatments.

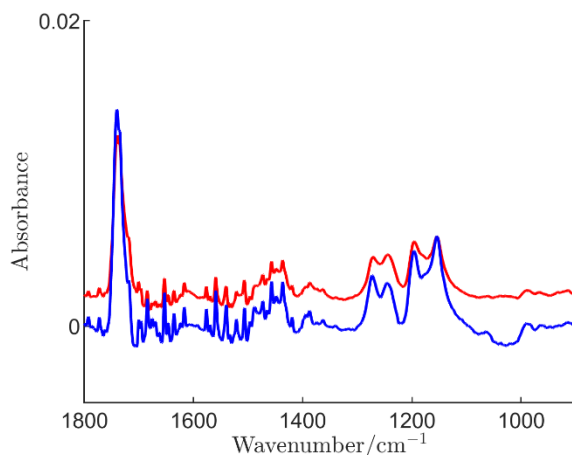


Figure S14. IRRAS spectra of $\text{GC}_{\text{Cat-PMMA}}$ ($\text{pH} = 7$) before (blue) and after (red, offset by 0.002 abs units) sonication in acetone for 20 min.

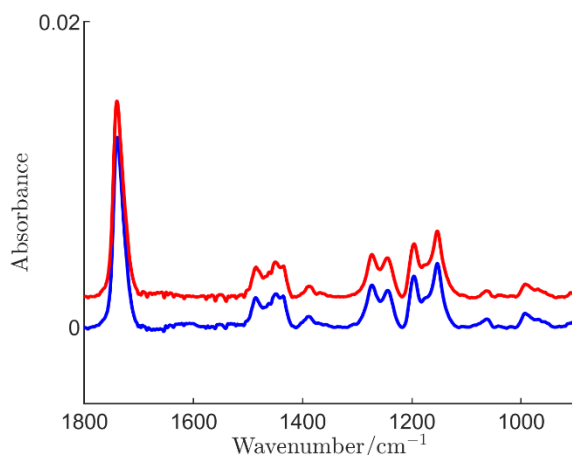


Figure S15. IRRAS spectra of $\text{GC}_{\text{Cat-PMMA}}$ ($\text{pH} = 7$) before (blue) and after (red, offset by 0.002 abs units) heating to $100\text{ }^{\circ}\text{C}$ for 1 h.

Electrochemical oxidation of GC_{PMMA} and $\text{GC}_{\text{Cat-PMMA}}$ (pH 8.3 and 10). These samples displayed a much smaller response to oxidation than $\text{GC}_{\text{Cat-PMMA}}$ (pH 7), leaving signals originating from the PMMA polymer brush after the oxidative treatment (Figures S16–S18). On GC_{PMMA} the thickness changed from 87 to 79 nm upon oxidation. The lack of response is due to the formation of non-responsive and permanently attached ATRP initiators. On samples $\text{GC}_{\text{Cat-PMMA}}$ (pH 8.3 & 10), ellipsometry measurements of the dry state film thickness before and after oxidation gave 67 and 58 nm ($\text{GC}_{\text{Cat-PMMA}}$ (pH 8.3)) and 70 and 29 nm ($\text{GC}_{\text{Cat-PMMA}}$ (pH 10)), respectively, showing incomplete polymer brush removal.

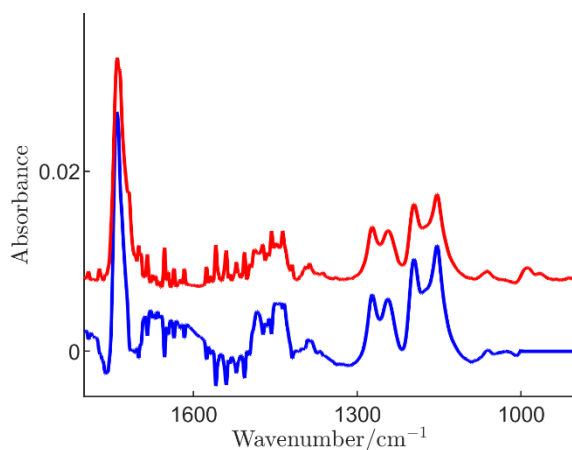


Figure S16. IRRAS spectra of $\text{GC}_{\text{Cat-Dopa-PMMA}}$ ($\text{pH} = 8.3$) before (blue) and after (red, offset by 0.008 abs units) electrochemical oxidation, consisting of three voltammetric cycles from -0.1 – 1.4 V vs SCE using $\nu = 0.1\text{ V s}^{-1}$ followed by a potentiostatic oxidation at 0.8 V vs SCE for 30 s. Signals between 1500 and 1700 cm^{-1} are due to changes in the concentration of water vapor in the chamber between recording of background spectra and sample spectra.

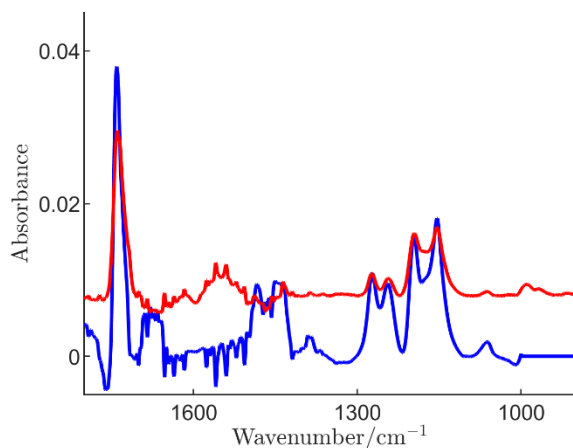


Figure S17. IRRAS spectra of **GC_{Cat}-PMMA (pH = 10)** before (blue) and after (red, offset by 0.008 abs units) electrochemical oxidation, consisting of three voltammetric cycles from -0.1 – 1.4 V vs SCE using $\nu = 0.1$ V s⁻¹ followed by a potentiostatic oxidation at 0.8 V vs SCE for 30 s. Signals between 1500 and 1700 cm⁻¹ are due to changes in the concentration of water vapor in the chamber between recording of background spectra and sample spectra.

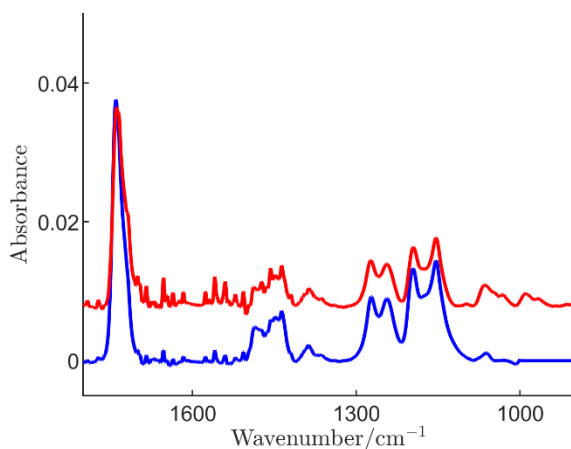


Figure S18. IRRAS spectra of **GC_{PMMA}** before (blue) and after (red, offset by 0.008 abs units) electrochemical oxidation, consisting of three voltammetric cycles from -0.1 – 1.4 V vs SCE using $\nu = 0.1$ V s⁻¹ followed by a potentiostatic oxidation at 0.8 V vs SCE for 30 s. Signals between 1500 and 1700 cm⁻¹ are due to changes in the concentration of water vapor in the chamber between recording of background spectra and sample spectra.

References

- S1. Jensen, M. T.; Ronne, M. H.; Ravn, A. K.; Juhl, R. W.; Nielsen, D. U.; Hu, X. M.; Pedersen, S. U.; Daasbjerg, K.; Skrydstrup, T., Scalable carbon dioxide electroreduction coupled to carbonylation chemistry. *Nat Commun* **2017**, *8*, 489.
- S2. Salehzadeh, H.; Nematollahi, D.; Khakyzadeh, V.; Mokhtari, B.; Henderson, L. C., General approach for electrochemical functionalization of glassy carbon surface by in situ generation of diazonium ion under acidic and non-acidic condition with a cascade protocol. *Electrochimica Acta* **2014**, *139*, 270-280.
- S3. Buhl, K. B.; Moller, R. K.; Heide-Jorgensen, S.; Kolding, A. N.; Kongsfelt, M.; Budzik, M. K.; Hinge, M.; Pedersen, S. U.; Daasbjerg, K., Highly Efficient Rubber-to-Stainless Steel Bonding by Nanometer-Thin Cross-linked Polymer Brushes. *ACS Omega* **2018**, *3*, 17511-17519.
- S4. Laviron, E., General Expression of the Linear Potential Sweep Voltammogram in the Case of Diffusionless Electrochemical Systems. *Journal of Electroanalytical Chemistry* **1979**, *101*, 19-28.